Physical and Chemical characterization of colloidal floc systems.

A thesis submitted towards partial fulfillment of
BS-MS Dual Degree Programme

by

Aparna Pilli

under the guidance of

Dr. Venkatesh Shankar

Senior Research Scientist, Unilever R & D, Bangalore

Indian Institute of Science Education and Research
Pune

Certificate

This is to certify that this thesis entitled "**Physical and Chemical characterization of colloidal floc systems**" submitted towards the partial fulfillment of the BS-MS dual degree programme at the Indian Institute of Science Education and Research Pune represents original research carried out by Aparna Pilli at Unilever R& D, Bangalore, under the supervision of Dr. Venkatesh Shankar during the academic year 2013-2014.

Student
Aparna Pilli

Supervisor
Dr.Venkatesh Shankar

Declaration

I hereby declare that the matter embodied in the thesis entitled **"Physical and Chemical characterization of colloidal floc systems"** are the results of the investigations carried out by me at Unilever R&D, Bangalore under the supervision of **Dr. Venkatesh Shankar,** R&D, Bangalore and the same has not been submitted elsewhere for any other degree.

Student
Aparna Pilli

Supervisor
Dr. Venkatesh Shankar

Acknowledgements

I would like to offer my profoundest gratitude to my thesis advisor, Dr. Venkatesh Shankar for offering his excellent guidance, support and patience without which I would not have been able to complete my thesis. In addition to academic mentoring, Dr. Venkat has worked a great deal in bringing out the best in me by encouraging me to be more proactive. I consider myself fortunate to be associated with him who has given a decisive turn to my career.

I would also like to thank all my lab members for providing me with an excellent atmosphere to work on my thesis. I got to learn a lot from their research experiences. Special thanks to PrasanthCS, Uma Madhavan, Manu George and Arindam Roy for their valuable inputs and great help in running the experiments.

Last but not the least, I would like to express my sincere gratitude to my family who have always encouraged and supported me in my constant pursuit for knowledge and learning.

Abstract

One of the most pervasive problems afflicting people throughout the world is inadequate access to clean drinking water. With water scarcities occurring globally, efforts are being made to increase pure water supply and safe re-use of wastewater. Addressing these problems calls out for a tremendous amount of research involving disinfection and decontamination of water. Lot of science and technology has been developed in order to identify robust methods of purifying water at lower cost and less energy, while at the same time minimizing the use of chemicals and impact on the environment. One such method of effective water purification is coagulation-flocculation followed by disinfection.

The removal of contaminants from effluents involves a process of flocculation and coagulation. Addition of specific chemicals changes the surface property of colloidal particles so as to facilitate the separation of solids from the solid-liquid interface. These colloids which come out of the suspension are called flocs or flakes. A systematic study of flocculation would include physical and chemical characterization of floc structures.

In this thesis, we have tried to address how the structure of floc can change as a function of pH, total dissolved solids, settling time and stirring speed. This was achieved by concentrating on fractal dimension changes, primary floc size and floc microstructure. Fractal concepts provide a new way of describing floc geometry and various physical properties such as density, porosity and settling velocity. The results have confirmed the direct relation between fractal dimension and floc compactness and floc behavior at different stirring speeds.

Chemical characterization primarily looked into the distribution of inorganic species on the surface and the active chemical organic groups. This was done at different pH and TDS (total dissolved solids) conditions and varied turbidity values of the solution. Characterization was done using Infrared and Raman Spectroscopy, EDX and XPS methods. It was observed that the inorganic species in the floc is covered by multiple layers of organic PAM and clay.PAM network formation and subsequent bridging mechanism was confirmed by imaging techniques.

LIST OF FIGURES

Table of Contents

Chapter 1

Introduction to Coagulation and Flocculation:

Clean, safe water is vital for everyday life. Water is essential for health, hygiene and the productivity of our community. Main sources of water are surface water, which includes lakes, rivers and fresh water wetlands, groundwater and Underflow Rivers. Natural water contains a wide range of impurities mostly arising from weathering of rocks and soils. Added to this, contributions from human activities, such as domestic and industrial wastes make water unfit for consumption, laundry and other industrial purposes. These impurities include inorganic particles such as clays and metal oxides, organic colloids, pathogenic microbes and dissolved natural organic matter. Many contaminants can be dangerous and necessary treatment is done to meet the "Drinking water quality standards" set by WHO [1].Others are removed to improve the water's smell, taste, and appearance.

Many methods are used for water purification but the most common method is coagulation and flocculation. This method of treatment involves less energy and is cost effective. It requires minimum use of chemicals and produces less sludge thus having little impact on the environment. Coagulation-Flocculation process is followed by sedimentation, filtration and disinfection.

Purification methods are chosen based on the size of impurities present. Particulate contaminants of the size beyond 1 μm can be removed easily by sedimentation and filtration techniques whereas those smaller than 1 μm are called colloids. Colloids carry charges on their surface and hence cannot be separated by conventional physical methods like sedimentation. Such a state of the suspension where particles are microscopically dispersed through a continuous phase is called stable state. Neutralization of charges on colloids and subsequent agglomeration is called de-stabilization or coagulation.

Flocculation is a process by which colloids form lager form larger agglomerates and undergo phase separation from the water system. This is achieved by the addition of a flocculant when the

colloids come out of the suspension in the form of flocs or flakes. In this thesis, hydrated aluminium salt and polyacrylamide were used as a flocculants.

1.1 Literature Survey

Although flocculation in the context of water purification dates back to early 19^{th} century [2], usage of alum coagulants for waste water treatment began from the late 20^{th} century [3].

Characterization of flocs is essential for the comprehensive study of coagulation-flocculation mechanisms. In earlier studies, the Smoluchowski equation [4,5]was formulated based on the assumption that floc aggregates are impermeable spheres. Recent studies have shown that flocs consist of multi-branched structures. Fractal concepts have provided a new way of describing floc geometry and various other physical properties such as density, porosity and settling velocity [6-10].However, influence of parameters such as TDS (total dissolved solids)or pH on the flocculation process has not been addressed. The main aim of this thesis was to test how flocs withstand extreme pH and TDS conditions. This was achieved by measuring dimension of flocs. Floc formation, growth and breakage and the influence of shear on the compactness of the floc have been studied.

Although physical characterization of flocs has been addressed to some extent in the earlier studies [11-13], no significant research has been done to study the surface chemical speciation during flocculation process. In this thesis, distribution of inorganic chemicals and organic species on the surface of floc was discussed. Infrared and Raman spectra were used to study the surface distribution of chemicals and bulk characterization was done using Energy dispersive X-ray spectroscopy and X-ray photo-electron spectroscopy.

Most interesting results were observed when imaging of dried flocs was done. The top view of floc showed a web like network of Polyacrylamide entrapping clay and rest of the colloids. This observation provided an experimental proof for the “bridging mechanism” of Polyacrylamide. Bright field microscope and Digital microscope were used for optical imaging.

1.2 Coagulation and Flocculation

Two chief forces acting on colloids are attractive Van der Waals forces and repulsive electrostatic forces [15]. Van der Waal's attractive force is directly proportional to the size of the particle and inversely proportional to the square of the distance between them. Electrostatic repulsion is the principle mechanism involved in controlling the stability of colloidal suspensions. The absorbed water molecules provide a liquid barrier preventing collisions and agglomeration and thus destabilization. Particles may acquire surface charges due to unequal distribution of constituent ions on the particle surface, preferential adsorption of specific ions, ionization of surface groups, crystal imperfection, or any combination of these.

1.3 Electrical double layer and Zeta potential

Oppositely charged ions in an electrolytic solution are attracted to the surface of the charged colloid [16]. The two opposing forces, electrostatic attraction and ionic diffusion, produce a diffuse cloud of ions surrounding the particulate, which can extend up to 300 nm [17].This co-existence of original charged surface and the counter-ions is known as electrical double layer. The double layer consists of two major regions, an inner layer (called Stern layer) where the initial layer of adsorbed ions and molecules are located at the particle surface; and the outer layer (called Gouy-Chapman layer) of oppositely charged counter-ions. The stability of colloidal suspension is greatly influenced by the potential of the Stern layer, which is generally referred to as the Zeta potential [18].

A charged particle dispersed in an ionic medium tends to have a concentration of opposite ions attracted towards it. For example, a negatively charged particle collects a number of positive counter-ions. As one move further away from the particle, concentration of counterions decreases due to diffusion until ionic equilibrium is reached. A plot of the charge contributed by these ions versus distance from the particle surface (Figure 1) reveals the familiar exponential decay. Now, if the particles were imagined to be moving, it would tend to drag its counterions along with it while leaving behind the ions that are further away from its surface. This would set up a plane of shear – the potential difference at which is called the zeta potential (ζ).Two models have been proposed for understanding the electric double layer; Goy-Chapman model and Stern model.

1.3.1 Gouy-Chapman model

Gouy-Chapman model [19] states that the distribution of charged colloidal particles in an electric field is determined by the balance between the thermal motion of ions and electrostatic interactions. In this model, the charge distribution of ions as a function of distance from the metal surface allows Maxwell–Boltzmann statistics to be applied.

$$n_i\,(x) = n_{oi}\, e^{\frac{-ze\psi(x)}{kT}} \tag{1.1}$$

where n_i: concentration of ions *i* (number of ions per unit volume)

n_{oi} : concentration of ions *i* in the bulk

z_i: valence (charge) of ions *i*

Ψ(x): electric potential, x= distance from the surface of colloid, T: absolute temperature

e: elementary charge (1.6 x 10^{-19} C), k: Boltzmann constant (1.38 x 10^{-23} J/K)

The dependence of electric potential on the distance to the surface is given by the Poisson equation:

$$\frac{d^2\Psi(x)}{d\,x^2} = -\frac{\rho(x)}{\varepsilon_0\varepsilon_r} \tag{1.2}$$

where the charge density at x is given by: $\rho(x) = e\,\Sigma z_i n_i(x)$

ε_o: dielectric constant of vacuum= 8.85 × 10^{-12} $C^2/(N\cdot m^2)$

ε_r: relative dielectric constant of the medium

The combined Poisson-Boltzmann equation is given by:

$$\frac{d^2\Psi(x)}{d\,x^2} = -\frac{e}{\varepsilon_0\varepsilon_r}\sum_i z_i\, n_{i0} \exp\left(\frac{-z_i e\Psi(x)}{kT}\right) \tag{1.3}$$

In general, Poisson-Boltzmann equation has to be solved numerically. For low electric potentials, ($ze\Psi << kT$). This gives an approximation to Poisson-Boltzmann equation called **Debye-Hückel approximation.** Applying this approximation to the above equation leads to a linearized form of Poisson-Boltzmann equation:

$$\frac{d^2\Psi(x)}{d\,x^2} = \kappa^2\Psi(x) \tag{1.4}$$

where

$$\kappa = \sqrt{\frac{\sum_i z_i^2 e^2 n_{i0}}{\varepsilon_0\varepsilon_r kT}}$$

κ^{-1} is called Debye length which is approximately equal to the thickness of double layer.

The solution to the above ordinary differential equation for electric potential is given by:

$$\Psi(x) = \Psi_0 \exp(-\kappa x) \tag{1.5}$$

where ψ_o= electric potential at the surface of the colloid

1.3.2 Stern model

Gouy-Chapman model fails for highly charged double layers. The size of the ions is not considered. Hence stern model [20] was proposed. Adsorption of ions on the surface forms the stern layer and the potential at stern layer is called the stern potential. The Stern layer accounted for ions' finite size (as opposed to point charges in Gouy-Chapman model) and consequently ions' closest approach to the electrode is on the order of the ionic radius. The Stern model had its own limitations- assuming that all significant interactions in the diffuse layer are Columbic, assuming dielectric permittivity to be constant throughout the double layer and that fluid viscosity is constant above the slipping plane.

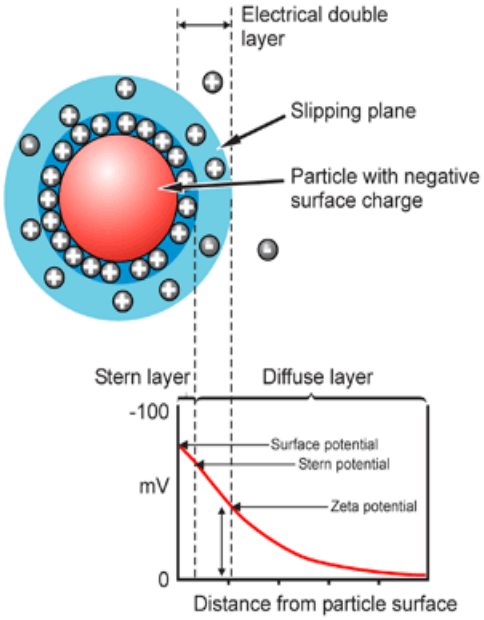

Figure 1: Electric double layer and Zeta Potential

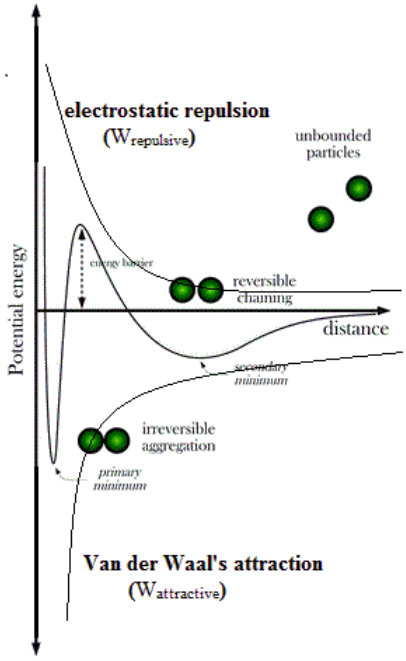

Figure 2: DLVO theory

1.4 Flocculation Mechanisms:

1.4.1 Charge neutralization

The original colloidal particles are negatively charged and hence positively charged ions from the coagulant get attracted to them. This deposition process results in charge neutralization. Charge neutralization [21, 22] by double layer compression is accomplished when flocculation is effective through an increase in solution ionic strength.

Electric double layer interaction energy per unit area is repulsive in nature and is given by:

$$W(x) = \frac{64\,\pi kTR\,n_o\phi_o^2}{\kappa^2} e^{-\kappa x} \quad (1.6)$$

where ϕ_o: reduced surface potential = $\tanh\left(\frac{ze\psi_o}{4kT}\right)$ and κ^{-1} = debye length

Since the double layer thickness is approximated by 1/κ, increase in ionic strength (I) decreases the thickness of the double layer.

$$\text{Ionic strength (I)} = \frac{1}{2}\,\Sigma\, z^2_i\, c_{i0} \quad (1.7)$$

(where c_{i0} = concentration of ions in the bulk) and $\kappa \propto \sqrt{I}$ (1.8)

This compression allows the approach of the colloidal particles to where short-range attractive forces predominate over electrostatic repulsive forces. In the presence of hydrolysable metal ions such as $Al^{3+}$and Fe^{3+}or polyelectrolytes of opposite charge to colloid surface, the charge is neutralized by adsorption of these species onto the particle surface and consequently double layer repulsion is reduced allowing aggregation to occur. Optimum flocculation occurs at the point of total charge neutralization i.e. when zeta potential will be zero.

1.4.2 DLVO theory

According to Deryagin and Landau [23, 24], Verwey and Overbeek, if the kinetic energy of the particle is large enough to surmount the potential hump created between them by way of double layer formation, the particles would coalesce otherwise they would remain as a stable suspension. This theory is popularly known as DLVO theory. It describes the balance between two forces, electrostatic repulsion and van der Waals attraction. Electrostatic repulsion becomes significant when two colloids approach each other and their electrical double layers begin to interfere. Some energy is required to overcome this repulsive force. The repulsion curve in

Figure 2, indicates the energy that must overcome if the particles are forced together. It has a maximum value, which is related to the surface potential, when they almost touch and decrease to zero outside the double layer. DLVO theory explains the tendency of colloids to agglomerate or separate by combining two curves of electrostatic repulsion and van der Waals attraction. At each distance, a smaller value is subtracted from the larger value to obtain the net energy. In the regime where there is repulsion, the potential hump can be described as energy barrier. We can increase or decrease the energy barrier by changing the ionic or pH environment or adding surfactants to affect the surface charge of the colloid.

Interaction potential energy (W) between two colloids or surfaces is given by

$$W_{total} = W_{attractive} + W_{repulsive} \quad (1.9)$$

where $W_{attractive}$ is Van der Waals energy and is different for different morphologies.

$W_{repulsive}$ is the electro-osmotic repulsion energy.

1.4.2.a Attractive interactions

Van der Waal's force is actually the total name of dipole-dipole force, dipole-induced dipole force and dispersion forces, in which dispersion forces are the most important part because they are always present. Assume that the pair potential between two atoms or small molecules is purely attractive and of the form $W = -C/r^n$, where C is a constant for interaction energy, decided by the molecule's property and n = 6 for van der Waals attraction.

In case of two flat plates, the net van der Waals energy per unit area is given by

$$W(x) = -\frac{A}{12\pi x^2} \quad (1.10)$$

where A = Hamakar constant, x = distance of separation between the plates

But colloidal particles have spherical geometry. In order to get the interaction energies between a pair of atoms or molecules [25], Derjaguin approximations (DA) have been used. DA procedure relates the interaction energy per unit area E between two flat plates and the interaction energy between two curved surfaces *U*.

$$U(D) \sim \int_A E(x)dA \sim f([r_1],[r_2]) \int_x^{\infty} E(x)dx \quad (1.11)$$

where D = distance of closest approach between the two curved surfaces

E(x): interaction energy per unit area between two infinite flat plates

x: distance of separation

d*A* is the differential area of the surfaces facing each other

[*r*1] and [*r*2]: the sets of the two principal radii of curvature of surfaces 1 and 2 at the distance of closest approach

f([r_1],[r_2]): a function of the radii of curvature of the surfaces.

One should note that for a spherical particle the two principal radii of curvature are identical. Two assumptions lead to the above expression. First, the range of the interaction energy is considered much shorter than the radii of curvature of the particles. This implies that the entire interaction energy between the two particles arises from a small region of the particles in the vicinity of the distance of closest approach, thus enabling the extension of the upper integration limit in equation to infinity. Furthermore, this assumption allows us to neglect higher order curvature effects in writing the final form of equation. Consequently, the function *f([r_1],[r_2])* represents curvature effects that are valid only near the distance of closest approach.

The second assumption underlying DA is related to the interpretation of the interaction energy per unit area between two infinite flat plates. The interaction energy per unit area is ideally defined as the interaction energy at any point on one of the flat surfaces due to the entire second flat plate. When using DA for two curved surfaces, the interaction energy per unit area between two infinite flat plates is conveniently defined as the interaction energy between two similar area elements on the opposing plates directly facing each other.

Thus in case of spherical particles, the net van der Waals interaction is given by;

$$F(x) = -\frac{AR_{eff}}{12x^2} \quad \text{and} \quad W(x) = -\frac{AR_{eff}}{12x} \tag{1.12}$$

Where $R_{eff} = \frac{r_1 r_2}{r_1 + r_2}$

1.4.2.b Repulsive interactions

When two charged surfaces or particles approach each other, their corresponding electrical double layers overlap. The accumulation of ions due to the overlap of the electrical double layers creates an increase in osmotic pressure. Water from the bulk comes to dissolve the accumulation of ions, preventing the surfaces from approaching closer. This is called **electro-osmotic double layer repulsion** [26].

$W_{repulsive}$ is the electric double layer repulsion which is given by:

$$W_{repulsive} = \frac{64\pi T}{\kappa^2} R_{eff}\, n_0\, \phi_0^{\,2}\, e^{-\kappa x} \qquad (1.13)$$

where ϕ_0 : reduced surface potential = $\tanh\left(\frac{ze\psi_o}{4kT}\right)$, κ^{-1} = debye length, T = absolute temperature,

$R_{eff} = \frac{r_1 r_2}{r_1 + r_2}$

The electro-osmotic double layer repulsion depends on the surface charge (σ_0, ψ_0), salt concentration, valence ions, radii of the particles, dielectric constant of the medium and temperature.

1.4.3 Bridging mechanism

Long chain polymers when added in small dosage to a suspension of colloidal particles, adsorb onto them in such a manner that an individual chain can become attached to two or more particles thus "bridging" [27] them together. This phenomenon is observed up to a particular optimum polymer dosage beyond which flocculation diminishes, a process being known as steric stabilization. The essential requirements for polymer bridging are that there should be sufficient unoccupied particle surface for attachment of polymer segments from chains attached to other particles and that the polymer bridges should be of such an extent that they span the distance over which inter-particle repulsion prevails. Thus, at lower dosages, there is insufficient polymer to form adequate bridging links between particles. With excess polymer, there is no longer enough bare particle surface available for attachment of segments and the particles become destabilized, which may involve some steric repulsion. On average, bridging flocculation gives aggregates (flocs) which are much stronger than those produced by addition of salts (i.e. by reduction in electrical repulsion). However, such stronger flocs produced by the bridging mechanism may not reform once broken at high shear rates.

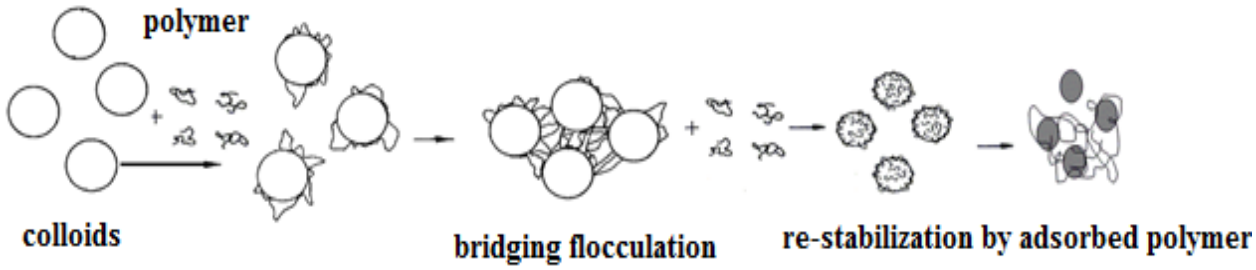

Figure 3: Bridging Mechanism

Chapter 2

THEORY

Physical Characterization of flocs was primarily focused on finding the fractal dimension and particle size of colloidal flocs. Recent studies have shown that flocs consist of multi-branched structures or fractals [28] that are not consistent with the floc structure described by classical Euclidean geometry.

2.1 Fractal dimension

Fractal dimension can be defined as a ratio providing a statistical index of complexity. It compares how the detail in a pattern changes with the scale at which it is measured. It has also been characterized as a measure of the space-filling capacity of a pattern but it is not equivalent to density. It can be expressed as:

$$\text{Fractal dimension} = \frac{detail\ in\ the\ pattern}{scale\ of\ measurement} \tag{2.1}$$

For ordinary geometric shapes, the theoretical fractal dimension is equal to the Euclidean or topological dimension. Thus, D_f is 0 for zero dimensional objects, 1 for one dimensional objects and so on. D_f is 2 for two dimensional surfaces and 3 for solids.

If we take an object having Euclidean dimension D and reduce its linear size by 1/r in each spatial direction, its measure i.e. length, area or volume, would increase to $N=r^D$ times the original [29]. (Figure 4)
On considering $N=r^D$, and taking log of both sides, we get:

$$\log N = D.\log r \tag{2.2}$$

Solving for D:

$$D = \frac{\log N}{\log r} \tag{2.3}$$

Here D is an integer for Euclidian geometry. If D is a fraction, it is called fractal dimension.

Fractals are typically self-similar patterns with an infinite nesting of structure at all scales. A fractal is one that has a fractal dimension that usually exceeds its topological dimension. Typical example of fractals is the Koch Curve.

In order to explain fractal dimension we consider a straight line of length 1 unit, called the initiator. We remove the middle one-third of the line, and replace it with two lines each having the same length (1/3 of the original) as the remaining lines on each side, and call it the generator. (Figure 5)

Since a line in the Koch Curve breaks up into 4 smaller pieces. Each of these pieces are 1/3 the length of the original. Therefore N is equal to 4 and r is equal to 3. Hence,

$$D_f = \frac{\log N}{\log r} \tag{2.4}$$

Which gives a fractal dimension of 1.26. This value is obviously greater than topological dimension which is a line which is 1.

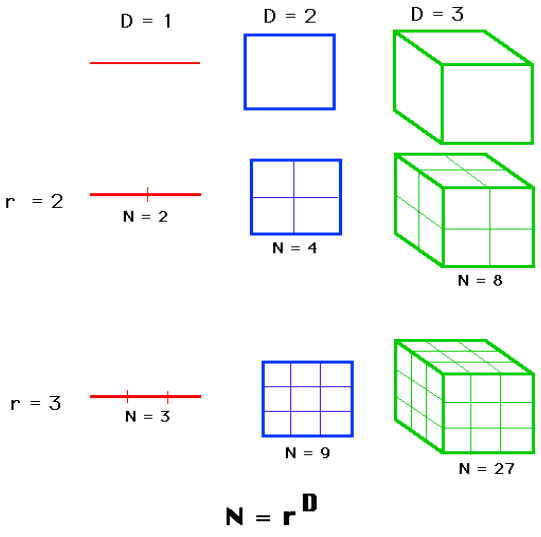

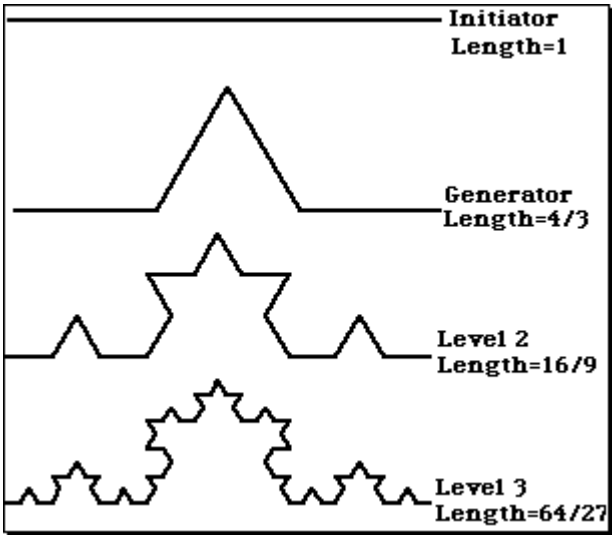

Figure 4: Geometrical shapes each reduced in size by 1/r **Figure 5: Koch Curve**

2.2 Mass fractal dimension

Floc structure is porous hence the same mass of floc spreads over a larger volume than a hard sphere of the same mass [30]. (Figure 6(a))

If M denotes floc mass and L denotes a characteristic measure of their size, then mass fractal dimension is given by:

$$M \propto L^{Df} \tag{2.5}$$

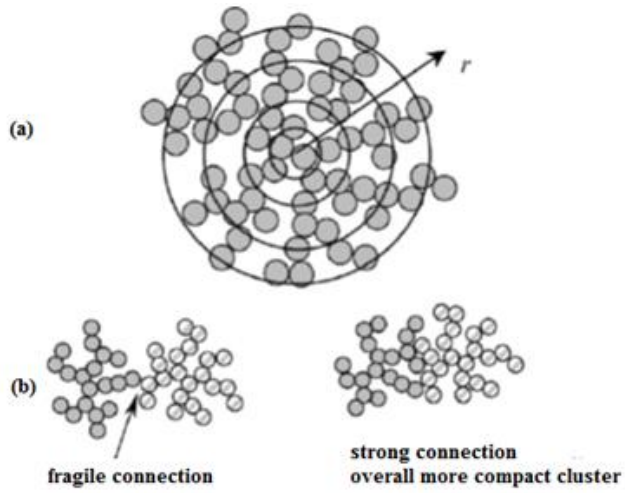

Figure 6(a): Variation of contained mass as a function of increasing radius

Figure 6(b): Effect of breakup and re-attachment leading eventually to stronger and compact aggregate structure associated with higher fractal dimension

2.3Compactness and floc strength

Compactness of floc is determined by fractal dimension values of floc (Figure 6(b)).A higher D_f value corresponds to a more compact interior floc structure [32].In case of compact aggregates, fractal dimension is found to lie in the range of 2.3 to 2.5 (or higher if "restructuring" occurs). For loose aggregates, it is in the range of 1.7 to 1.8 [40-41].

There is no straight forward technique to measure floc strength. Hence floc breakage mode can be defined as floc strength [31].

$$\mathbf{\log d = \log C - \gamma \log G} \tag{2.6}$$

where: d is floc diameter

G is the average velocity gradient in the flocculator

γ is an exponent of stable floc size (depends on floc break-up mode)

C is floc strength const. (depends on method used for floc size measurement)

The slope of the equation γ denotes the rate of degradation. The steeper the slope γ, more prone the flocs are to breakage under increasing shear rate.

Hence the value of γ is considered as an indicator of floc strength [32].

2.4 Effect of stirring speed on floc formation

An optimum speed of stirring must be maintained for flocs to form. Stirring too fast or too slow doesn't result in proper flocculation. Higher the speed of stirring, the aggregates reach equilibrium faster, followed by floc breakage. In case of aluminium flocs optimum stirring speed was found to be 70 rpm.

2.5 Infrared Spectroscopy

Molecular vibrations occur when atoms in a molecule are in periodic motion while the molecule as a whole has constant translational and rotational motion. The frequency of the periodic motion is known as a vibration frequency. The typical frequencies of molecular vibrations range from less than 10^{12} to approximately 10^{14} Hz which falls in the IR range.

A molecular vibration is triggered when the molecule absorbs energy equal to vibration's frequency, *v.* There are two types of molecular vibrations namely stretching and bending modes. Stretching modes include symmetric and asymmetric stretching while rocking, scissoring, wagging and twisting come under bending modes (Figure 7) IR spectroscopy is used in case of asymmetric vibrations i.e. when there is a change in the dipole moment [33].

$$E_n = h\left(n + \frac{1}{2}\right)\vartheta = h\left(n + \frac{1}{2}\right)\frac{1}{2\pi}\sqrt{\frac{k}{m}} \qquad (2.7)$$

where *n = quantum no. which can take values 0,1,2 …*

ϑ= *vibrational frequency*

v= vibrational quantum no. = $n+\frac{1}{2}$

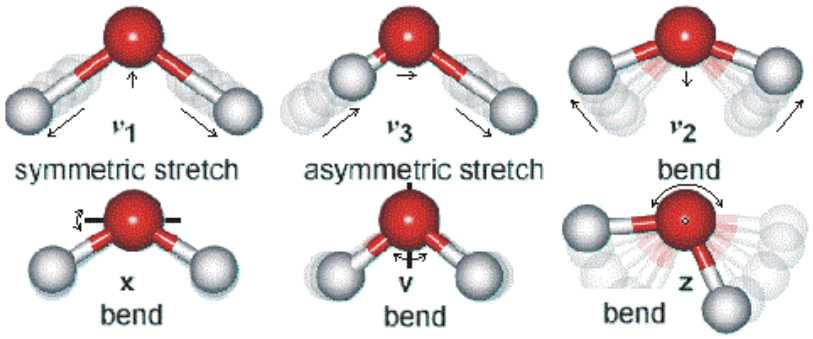

Figure 7: Molecular Vibration modes

2.6 Raman Spectroscopy

Raman scattering or Raman effect is the inelastic scattering of a photon. i.e. frequency of scattered photons is different from incident. Raman spectra is observed in molecules when there is change in the polarizability. It uses higher intensity laser with wavelengths in either the visible or near-infrared regions. Thus Raman spectroscopy is mostly used to detect symmetric vibrations in a molecule. Spatial charge separation under influence of electric field E, induced dipole moment μ and α is the polarizability [34], then

$$\mu(t) = \alpha(t)\, E(t) \tag{2.8}$$

If the incident radiation has frequency ω and the polarizability of the molecule changes between α_{min} and α_{max} at a frequency ω_{int} as a result of this rotation/vibration.

$$\mu(t) = (\alpha + \frac{1}{2}\Delta\alpha \cos\omega_{int}t)\, E_o \cos\omega t \tag{2.9}$$

Expanding this product yields:

$$\mu(t) = \alpha E_o \cos\omega t + \frac{1}{4}\Delta\alpha E_o\, (\cos\,(\omega + \omega_{int})t + \cos\,(\omega - \omega_{int})t) \tag{2.10}$$

where the first term denotes Rayleigh scattering, the second and third terms represent Anti-Stokes and Stokes scattering respectively.

2.7 Energy dispersive X-ray analysis

Energy-dispersive X-ray spectroscopy is an analytical technique used for the elemental analysis or chemical characterization of a sample. It relies on an interaction of some source of X-ray excitation and a sample. Its characterization capabilities are due in large part to the fundamental principle that each element has a unique atomic structure allowing unique set of peaks on its X-ray spectrum [35]. To stimulate the emission of characteristic X-rays from a specimen, a high-energy beam of charged particles such as electrons or protons, or a beam of X-rays, is focused into the sample being studied.

In the ground state of atom only certain orbital states with specific energies exist and these are defined by quantum numbers. With increasing Z, orbits are occupied on the basis of minimum energy, those nearest the nucleus, and therefore the most tightly bound, being filled first. Orbital energy is determined mainly by the principal quantum number (n). The shell closest to the nucleus (n = 1) is known as the K shell; the next is the L shell (n = 2), then the M shell (n = 3), etc. The L shell is split into three subshells designated L1, L2 and L3, which have different quantum configurations and slightly different energies (where as the K shell is unitary). Similarly, the M shell has five subshells. This model of the inner structure of the atom is illustrated in Figure 8.

The populations of the inner shells are governed by the Pauli Exclusion Principle, which states that only one electron may possess a given set of quantum numbers. The maximum population of a shell is thus equal to the number of possible states possessing the relevant principal quantum number. In the case of the K shell this is 2, for the L shell 8, for the M shell 18 etc.

The incident beam may excite an electron in an inner shell, ejecting it from the shell while creating an electron hole where the electron was. An electron from an outer, higher-energy shell then fills the hole, and the difference in energy between the higher-energy shell and the lower energy shell may be released in the form of an X-ray. The number and energy of the X-rays emitted from a specimen can be measured by an energy-dispersive spectrometer. As the energy of the X-rays is characteristic of the difference in energy between the two shells, and of the atomic structure of the element from which they were emitted, this allows the elemental composition of the specimen to be measured.

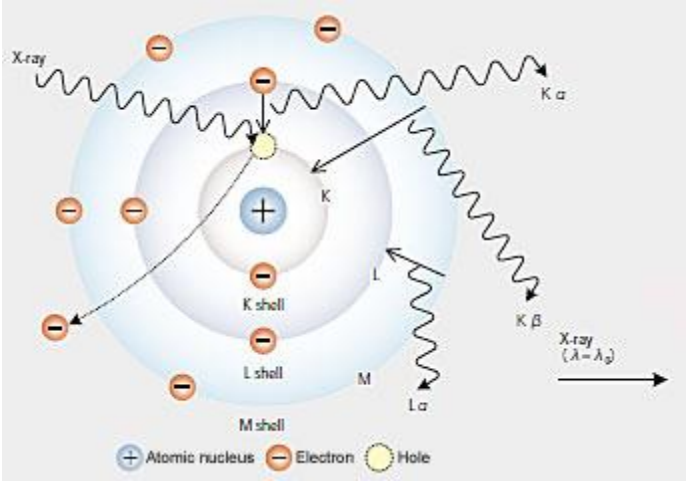

Figure 8:A model of the inner structure of the atom

2.8 X-ray photoelectron spectroscopy

X-ray photoelectron spectroscopy (XPS) [36] is a surface-sensitive quantitative spectroscopic technique that measures the elemental composition, empirical formula, chemical state and electronic state of the elements that exist within a material. XPS spectra are obtained by irradiating a material with a beam of X-rays while simultaneously measuring the kinetic energy (Figure 9 (a)) and number of electrons that escape from the top 0 to 10 angstroms of the material being analyzed. XPS requires high vacuum for sample preparation ($P \sim 10^{-8}$ Torr), before being transferred into the main analysis chamber which is in ultra-high vacuum ($P < 10^{-9}$ Torr) conditions. XPS although is a surface chemical analysis technique, can also be used to intentionally expose deeper layers of the sample in depth-profiling XPS, exposure to heat to study the changes due to heating, exposure to reactive gases or solutions, exposure to ion beam implant, exposure to ultraviolet light, to name a few.

Since the energy of an X-ray with particular wavelength is known (for aluminum $K\alpha$ X-rays, E_{photon} = 1486.7 eV), and the emitted electrons' kinetic energies are measured, the electron binding energy of each of the emitted electrons can be determined by using an equation that is based on the work of Ernest Rutherford:

$$E_{binding} = E_{photon} - (E_{kinetic} + \phi) \quad (2.11)$$

where $E_{binding}$ is the binding energy (BE) of the electron, E_{photon} is the energy of the X-ray photons being used, $E_{kinetic}$ is the kinetic energy of the electron as measured by the instrument and ϕ is the work function of the spectrometer (not the material).

This equation is essentially a conservation of energy equation. The work function term ϕ is an adjustable instrumental correction factor that accounts for the few eV of kinetic energy given up by the photoelectron as it becomes absorbed by the instrument's detector. It is a constant that rarely needs to be adjusted in practice.

A typical XPS spectrum is a plot of the number of electrons detected (sometimes per unit time) versus the binding energy of the electrons detected. Each element produces a characteristic set of XPS peaks at characteristic binding energy values that directly identify each element that exists in or on the surface of the material being analyzed. These characteristic spectral peaks correspond to the electron configuration of the electrons within the atom. The number of detected electrons in each of the characteristic peaks is directly related to the amount of element within the XPS sampling volume.

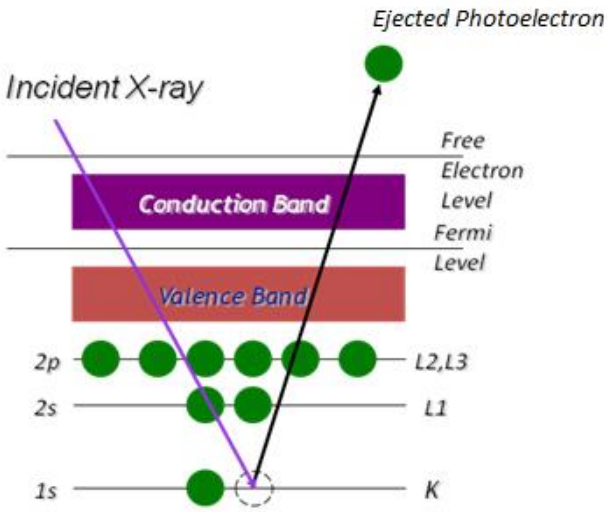

Figure 9: Photoelectron getting ejected upon irradiation with X-rays.

Chapter 3

MATERIALS AND METHODS

3.1 Sample Preparation

Samples with different parameters were prepared in a 2 litre beaker. To 1 litre de-ionized water, salts Magnesium chloride hexahydrate ($MgCl_2.6H_2O$), Calcium chloride dihydrate ($CaCl_2.2H_2O$) and Sodium bicarbonate ($NaHCO_3$) were added in the ratio of 1:2:4 in order to adjust the TDS to desired value. TDS is a measure of the combined content of all inorganic and organic substances contained in a liquid in molecular, ionized or micro-granular suspended form. It is used as an indication of hardness or softness of water (since it gives an estimate of the number of ions present in the suspension) and as an aggregate indicator of the presence of a broad array of chemical contaminants. The pH of the solution was maintained by adding dilute (0.1N) HCl and NaOH solutions.

Initial solution was prepared by adding 0.05 g of bentonite clay. Clay particles act as nuclei in the coagulation-flocculation process. Flocs are prepared by adding 0.1g of Aluminium Sulfate hexadecahydrate.

Bentonite clay acts as the nuclei for coagulation and flocs are generated using Aluminium Sulfate hexadecahydrate. Polyacrylamide was used as sweep flocculant and Sodium carbonate in order to adjust the basicity of solution.

3.2 Particle size measurement method

Particle size of flocs was measured using Malvern Mastersizer 2000 (Figure 10). This works on the principle of laser light diffraction. Due to its simplicity and accuracy, this method has been employed for the determination of particle size distribution in disperse systems. The measurement procedures on modern laser diffraction (LD) devices are fast, fully automated and reproducible.

The LD technique is based on the fact that the spatial distribution of scattered light is a function

of the particle size of the sample to be analyzed. Light diffraction is a phenomenon which occurs when an EM wave encounters an obstacle, here particle. The waves near the site of impact are more intense and decreases as one goes away from the particle [37]. Larger particles will create more waves which are more intense and clearly separated whereas smaller particles produce more diffusive diffraction images. LD method [38] measures the intensity of the diffraction rings and the distance between them (declination angles from the direction of incident light). Besides diffraction, other phenomena such as reflection, refraction, absorption and re-radiation also occur during the illumination of particles.

We are more interested in the scattered light. In contrast to diffracted light, which is emitted at small angles relative to incident light, scattering occurs in all directions. The special distribution of scattered light is called the scattering pattern of a particle.

The scattering pattern depends on the ratio of particle diameter D and the wave length of incident light λ. Thus the scattering pattern changes with the size of the particle and wavelength of incident light. Depending on $\frac{D}{\lambda}$ ratio, the scattering is called Mie, Fraunhofer or Rayleigh scattering.

Since detectors cannot detect if the scattered light is because of LD or some other phenomenon, Mie theory has been developed. Mie theory is a solution to Maxwell's equations which describes the scattering of electromagnetic radiation by a sphere. The solution takes the form of an analytical infinite series. Rayleigh scattering describes the elastic scattering of light by spheres which are much smaller than the wavelength of light. The Rayleigh scattering model breaks down when the particle size becomes larger than around 10% of the wavelength of the incident radiation. In the case of particles with dimensions greater than this, Mie's scattering model can be used to find the intensity of the scattered radiation. However Mie scattering differs from Rayleigh scattering in several respects; the intensity, *I*, of the Rayleigh scattered radiation depends on wavelength of light and is equal in both forward and reverse directions. Whereas Mie scattered intensity is roughly independent of wavelength and it is larger in the forward direction than in the reverse direction. The greater the particle size, the more of the light is scattered in the forward direction.

The Fraunhofer theory is one of the approximate expressions of the Mie scattering theory. This approximate expression can be used only when the particle size is relatively large (at least, 10 times the laser wavelength) and the scattering angle is small (30° or less).

Fraunhofer scattering intensity is greater than that of Mie or Rayleigh scattering. The scattering angle is comparatively small and the ratio of light scattered forward and backward is small in case of Mie than Fraunhofer scattering.

Mie solution giving the total scattered light intensity:

$$I(\theta) = E \{ k^2 D^4 [J1]^2 \theta + [K_1 \theta]^1 + [K_2 \theta]^3 + [K_3 \theta]^5 + k^4 D^6 (m-1)^2 \theta^6 / 8\pi \} \quad (3.1)$$

where I is the scattered light intensity, E is the flux of incident light per unit area, D is the particle diameter, J1 is the Bessel function of first order, θ is the scattering angle and m is the complex refractive index [37]. K, k are constants.

For the calculation of scattered intensities, we need particle diameter D, scattering angle (θ) and optical parameter m which is the complex refractive index. Scattering angle is measured by the detectors and corresponding D value is calculated.

Figure 10: Malvern Mastersizer 2000

3.3 Fractal dimension measurement method

Fractal dimension of flocs is measured using Malvern Mastersizer 2000. The mass of a fractal object of dimension *d* scales as $M(r) \sim r^d$ [30]. Here *d* is between 2 and 3 for a surface fractal in three-dimensional space. It is equal to 2 for a perfectly smooth surface, and approaches 3 for a highly folded/convoluted surface.

Scattering from a mass fractal is considered from the 3D Fourier transform of the scattering length distribution function [39], which now scales as

$$I(q) \sim \frac{1}{q}\int_0^{\infty} r^{d-2}\sin(qr)\ dr \tag{3.2}$$

where scattering vector q (Figure 11) is given by: $q = \frac{4\pi n \sin\left(\frac{\theta}{2}\right)}{\lambda}$ (3.3)

Here wavelength (λ) of red laser light is 632 nm and refractive index (n) for water is known.

This yields a scaling of

$$I(q) \sim q^{-d} \tag{3.4}$$

The slope of a log-log plot of intensity versus wave vector thus yields the fractal dimension of the object under study at a particular length scale.

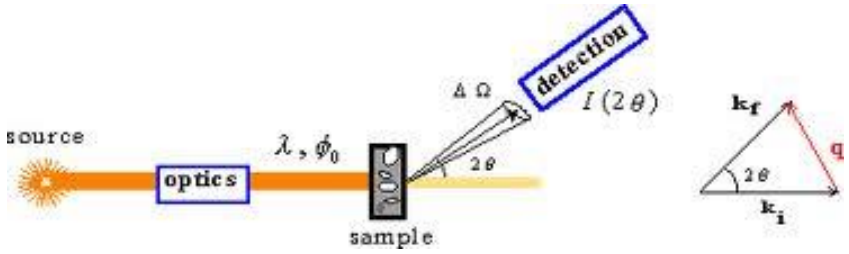

Figure 11: Light scattering by sample in Malvern Mastersizer. Here q represents scattering vector, k_i shows the incident wave and k_f represents elastically scattered wave.

3.4 Fourier Transform Infrared Spectroscopy

Chemical characterization of floc is done using FTIR technique. Different compounds have characteristic vibrations. To find the elemental distribution, dried floc sample was heated in the oven at 120 degrees for two hours in order to remove any leftover moisture and was stored in a vacuum desiccator. Potassium bromide standard, used for calibration of the instrument, is also kept in the oven at 120 degrees since any moisture content in the sample would result in a huge H_2O absorption peak at 3650 cm^{-1} which hinders the finger printing process. The dried floc

powder and the KBr standard are added in the ratio of 1:100 and ground into a fine powder for analysis.

The IR radiation is passed through a sample. Some of the infrared radiation is absorbed by the sample and some of it is passed through (transmitted). The resulting spectrum represents the molecular absorption and transmission, creating a molecular fingerprint of the sample. We have used *PerkinElmer* FTIR Spectrometer (Figure 12) and *Diffuse Reflectance Sampling Accessory* for spectral acquisition. Floc samples with varied turbidity values are analysed using this technique.

Figure 12: Fourier transform infrared spectrometer. Principle of working – Michaelson interferometry

3.5 Raman Spectroscopy

Raman spectroscopy is a technique used for elemental analysis and surface speciation of the sample. For molecules undergoing symmetric vibrations, IR spectroscopy cannot be used for characterization since dipole moment change is not observed. In such case Raman Spectroscopy is used for characterization.

Much sample preparation is not required for Raman analysis. This technique provides complimentary information to IR spectroscopy. We have used *Renishaw's inViaRaman Microscopy* for spectral acquisition. These microscopes support laser wavelengths from the near-infrared to deep ultraviolet.Calibration of Raman spectrometer is done using silicon calibration standard which gives a peak at 520 cm^{-1}. After calibration, the sample is mounted on a glass slide and adjusted to position using *ProScan* monitorized microscopic stage and Raman spectra is acquired. Floc samples with varied turbidity values are analysed using this technique.

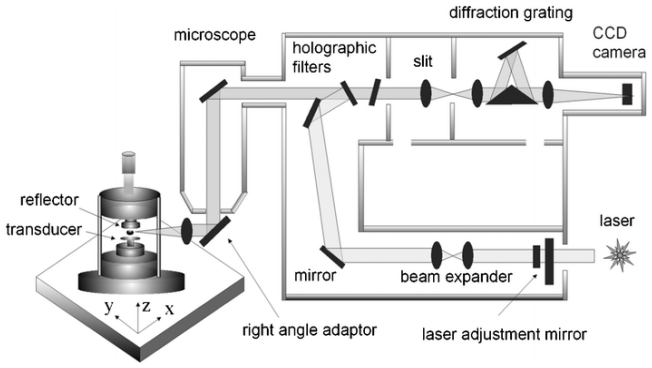

Figure 13: Raman microscope and instrumentation

3.6 Surface elemental composition and elemental analysis:

Three different floc samples are taken. Sample A: Floc made without adding Polyacrylamide. Sample B: Arizona dust is added in the floc formulation. Sample C: Floc with Polyacrylamide and no Arizona dust. Note that Arizona dust is added to increase the turbidity of the solution. Pellets of these samples of the size 1 cm x 1 cm x 2 mm are made using IR pelletizer- Hydrolic Pellet Press.

Energy dispersive and X-ray photoelectron spectroscopy were used for surface characterization and bulk chemical characterization respectively. Gold 4f was used for EDX calibration- Au $4f_{7/2}$ peak at 84 eV and Au $4f_{5/2}$ at 88 eV.

Figure 14: X-ray photoelectron spectroscope

Figure 15: Energy dispersive X-ray spectroscope

Chapter 4

RESULTS AND DISCUSSIONS

4.1Physical Characterization

Fractal dimension of flocs and particle size measurements were recorded using the particle sizer Malvern Mastersizer 2000 by varying different parameters.

4.1.1 Fractal dimension versus pH at constant TDS:

The TDS of the sample was kept constant and pH was varied from 5 to 8 and fractal dimension of the floc was recorded.

Table 1: *Fractal dimension values of samples at 60 ppm, 350 ppm and 700 ppm for a pH of 5,6,7,8.*

pH	D_f for 60 ppm	D_f for 350 ppm	D_f for 700 ppm
5	2.44	2.45	2.41
6	2.31	2.46	2.44
7	2.49	2.46	2.48
8	2.32	2.48	2.47

4.1.2 Fractal dimension versus TDS at constant pH:

The pH of the sample was kept constant and pH was varied from 5 to 8 and fractal dimension of the floc was recorded.

Table 2: *Fractal dimension values of samples at pH = 5,6,7 and 8 at constant TDS of 60, 350 and 700 ppm.*

TDS (ppm)	D_f for pH =5	D_f for pH =6	D_f for pH= 7	D_f for pH= 8
60	2.44	2.31	2.48	2.32
350	2.45	2.46	2.45	2.48
700	2.41	2.44	2.35	2.47

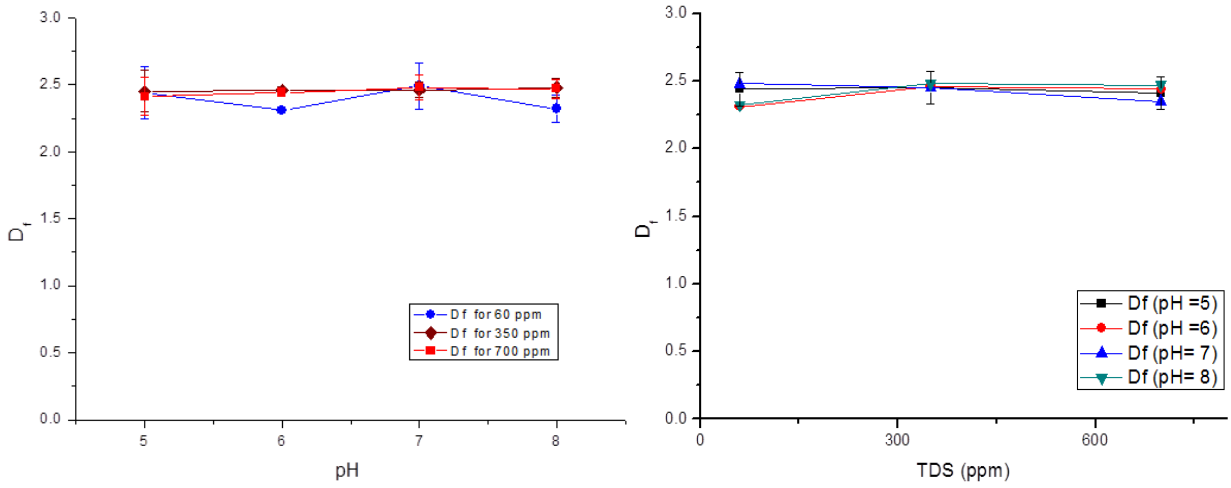

Figure 16 (a): D_f versus pH graph (at constant TDS) **Figure 16 (b):** D_f versus TDS graph at constant pH

Observations:

Fractal dimension remains almost constant upon changing pH or TDS values. Average fractal dimension is found to be2.44.

4.1.3 Change in the fractal dimension with time at increased shear

(a) Stirring at 70 rpm

Using the same formulation a sample was prepared keeping the pH and TDS constant at 7 and 700 ppm respectively. The floc sample was stirred at 70 rpm using Jar Test method and variation in fractal dimension with time was recorded.

Table 3: *Fractal dimension values of samples at pH = 5,6,7 and 8 at constant TDS of 60, 350 and 700 ppm.*

t (sec)	D_f
0	1.984
1.66	1.937
3	2.05
5	1.965
8	2.191
11	2.222
13	2.395
15	2.375
19	2.34
21	2.424

23	2.389
26	2.228
30	2.38
32	2.41
34	2.256
36	2.415
40	2.472

(b) Stirring at 150 rpm

Using the same formulation a sample was prepared keeping the pH and TDS constant at 7 and 700 ppm respectively. The floc sample was stirred at 150 rpm using Jar Test method and variation in fractal dimension with time was recorded.

Table 4: *Fractal dimension values of samples at pH = 5,6,7 and 8 at constant TDS of 60, 350 and 700 ppm.*

t (sec)	D_f
0	2.543
7	2.49
11	2.444
17	2.463
21	2.568
26	2.572
31	2.5
38	2.462
42	2.406

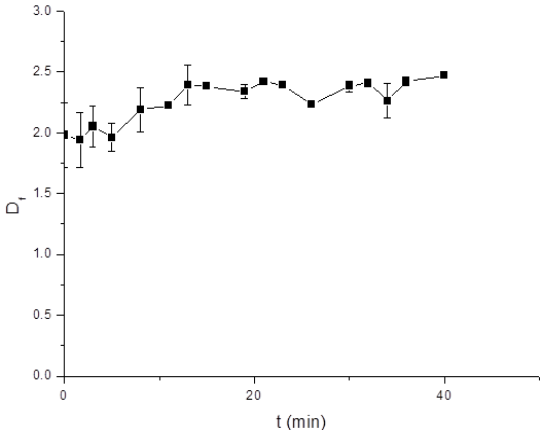

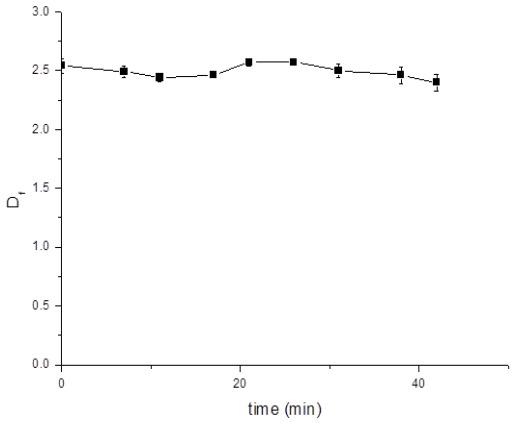

Figure 17 (a) : D_f versus time graph at constant stirring speed of 70 rpm

Figure 17 (b) : D_f versus time graph at constant stirring speed of 150 rpm

4.1.4 **Fractal dimension versus stirring speed [42]**

A sample with pH 7 and TDS 700 ppm was prepared and stirred initially at 173 rpm for 1.5 min using Jar test method(in order to mix the). Later the stirring speed was decreased to 40 rpm and fractal dimension (D_f) measurements were taken. Speed was then increased to 173 rpm for 24 min and D_f was recorded later. Finally the rate was brought back to 40 rpm and the D_f readings were taken.

An increase in fractal dimension from intial to final recording was observed. This indicates that the flocs have re-grown into more compact flocs.

Table 5: *For pH =7, TDS = 700 ppm*

t (min)	D_f
0	2.28
2	2.1
4	2.2
8	2.06
10	2.3
12	2.33
14	2.38
16	2.32
19	2.33
20	2.5
22	2.54
25	2.35
28	2.49
30	2.45
32	2.66

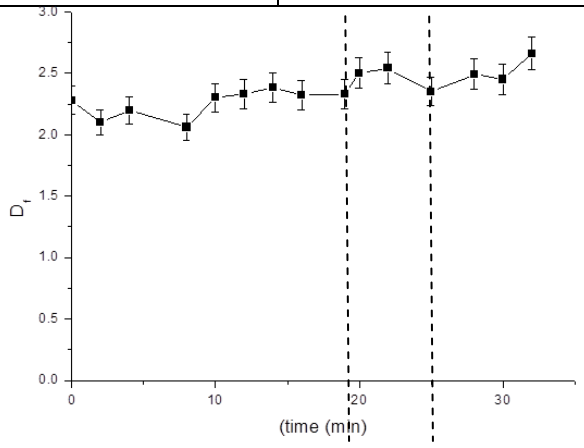

Figure 18: D_f versus time graph initially stirred at 40 rpm then 170 rpm followed by 40 rpm

4.1.5 Fractal dimension versus time for extreme pH, TDS values at a constant stirring rate of 70 rpm

Table 6: *Dynamic fractal dimension values for pH =5,8 and TDS = 60ppm, 700 ppm*

t (min)	D_f (pH =5, TDS =60ppm)	D_f (pH =8, TDS =60ppm)	D_f (pH =5, TDS =700 ppm)	D_f (pH = 8, TDS =700ppm)
0	1.88	1.79	2.06	1.97
1	-	1.77	-	-
2	-	-	2.06	-
3	2.54	-	2.11	-
4	2.59	2.04	-	-
5	-	-	2	2.17
6	2.51	-	-	-
7	-	-	2.07	2.28
8	2.53	-	-	-
9	-	2.36	2.12	2.38
10	2.55	-	-	-
11	2.58	-	-	2.38
12	-	-	2.12	-
13	2.54	-	2.07	2.3
14	-	2.42	-	-
15	2.49	-	2.16	2.31
16	2.54	-	-	-
17	-	-	2.26	2.38
18	-	-	2.15	-
19	2.46	2.43	-	2.17
20	2.5	-	2.26	-
21	-	-	-	2.15
22	2.38	-	2.35	-
23	-	-	2.37	2.09
24	2.42	2.57	-	-
25	-	-	2.23	2.18
26	2.38	2.31	-	-
27	-	-	2.15	2.2
28	2.37	2.28	-	-
29	-	-	2.13	-
30	2.38	-	-	2.14
31	-	-	2.26	-
32	2.39	2.23	2.21	-
33	-	-	-	-
34	2.31	2.2	2.28	-
35	-	-	-	-
36	2.33	2.2	2.15	-
37	-	-	-	-
38	2.29	-	2.26	-
39	-	2.13	-	-
40	2.3	-	-	-
41	2.3	-	-	-
42	-	-	-	-
43	2.27	-	-	-

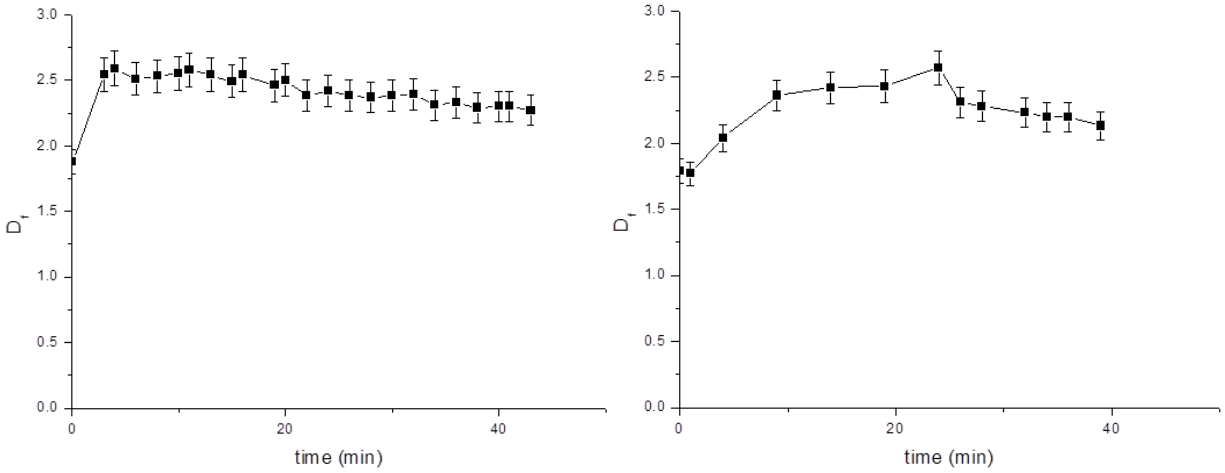

Figure 19 (a): D_f versus time graph at pH = 5, TDS = 60 ppm **(b)** At pH = 8, TDS = 60 ppm

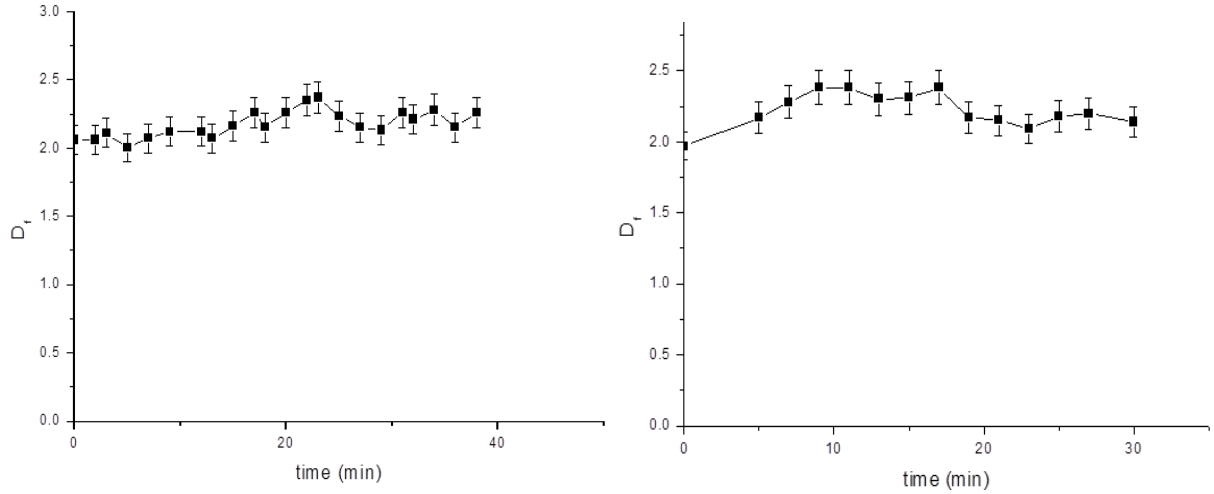

Figure 19 (c): D_f versus time graph at pH = 5, TDS = 700 ppm **(d)** At pH = 8, TDS = 700 ppm

Observations:

- For low pH (pH = 5) and low TDS (= 60 ppm): D_f increases very fast (to 2.59 at t= 4 min) and decreases gradually.
- For low pH (pH = 5) and high TDS (=700 ppm): flocs are not formed at all. D_f remains constant throughout.
- For high pH (pH = 8) and low TDS (= 60 ppm): D_f increases gradually (to 2.57 at t=24 min) and decreases gradually.
- For high pH (=8) and high TDS (=700 ppm): D_f increases gradually (to 2.38 at t=17 min) and decreases gradually.

4.1.6 Particle size variation with pH and TDS

a) The TDS of the sample was kept constant and pH was varied from 5 to 8 and the average particle size of the floc, d(0.5), was recorded using Malvern Mastersizer 2000. The observations were as follows:

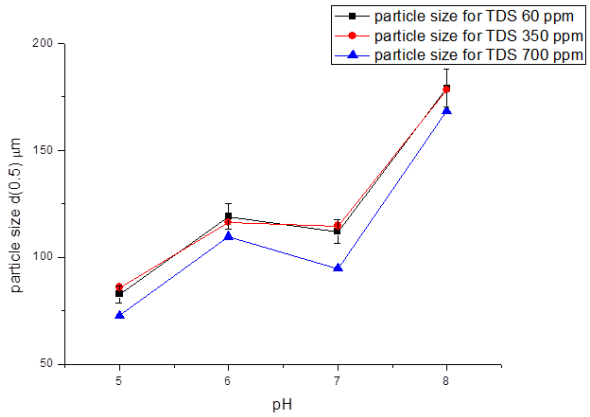

b) The pH of the sample was kept constant and TDS was varied to 60ppm, 350 ppm and 700 ppm. The average particle size of the flocd(0.5) was recorded using Malvern Mastersizer 2000. The observations were as follows:

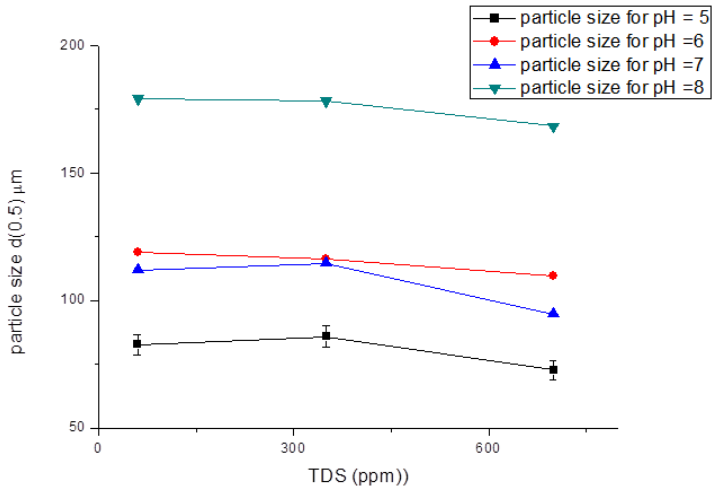

The results show that:

- Particle size is maximum at pH = 8 and it is almost equal for pH =7 and 6. Flocs show smallest sizes at pH = 5. This implies that flocs are barely formed at lower pH values
- Primary particle size of flocs remains invariant under TDS changes.

4.2Chemical Characterization

4.2.1 Infrared characterization:

Initially IR spectra of raw materials were recorded. This was followed by two floc formulations; one having 0 turbidity (i.e. no Arizona dust) and the other with turbidity 2.5 were sampled for IR characterization.

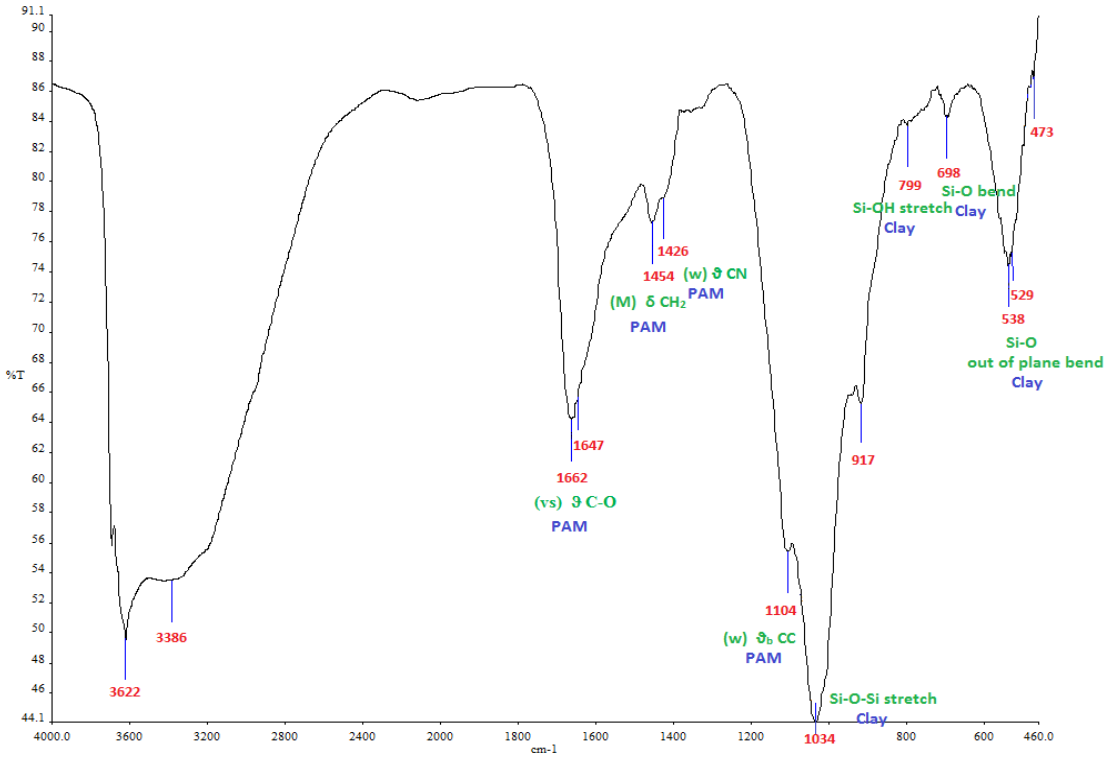

Figure 20 a,b: (Above) IR spectra of floc with 0 turbidity (no arizona dust). **(Below)** IR spectra offlocwith non zero turbidity

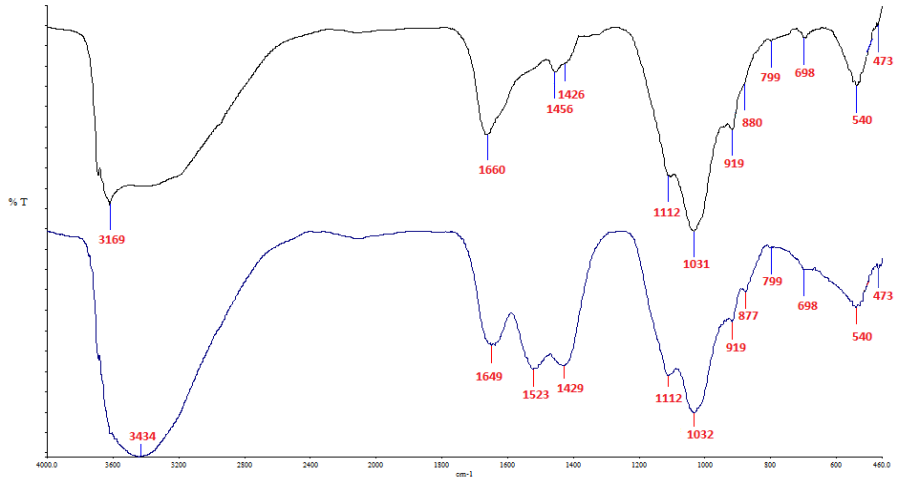

Table 7 : *IR characterization of raw materials*

Compound	Signature peaks
$Al_2(SO_4)_3$.$16H_2O$	1084 cm^{-1} (vs) ϑ3 (SO4) triply degenerate stretch
Polyacrylamide	1653 cm^{-1} (vs) ϑ C-O
$CaCl_2.2H_2O$	1633 cm^{-1}
$MgCl_2.6H_2O$	1633 cm^{-1}
Na_2CO_3	1454 cm^{-1} ϑ_3 symmetric stretching doubly degenerate

Upon comparing the floc spectra to that of the raw materials, it was observed that floc spectra showed only PAM and clay signature peaks. None of the added inorganic raw materials (i.e. aluminium, sodium, calcium, magnesium, silicates from bentonite clay) are seen.

On comparing the flocs with and without turbidity, it was observed that the two spectra match each other and both of them show only signature peaks of PAM and clay.

Hence we can conclude that PAM and clay have masked all the inorganic species in the floc surface.

4.2.2 Raman characterization:

Table 8: *Raman characterization of raw materials*

Compound	Signature peaks
$NaHCO_3$	1044 cm^{-1} , 1516 cm^{-1} OH bending
$Al_2(SO_4)_3$.$16H_2O$	467 cm^{-1} ϑ_2 , 611 cm^{-1} ϑ_4, 911 cm^{-1} ϑ_1
Polyacrylamide	1000 cm^{-1} C-C ϑa, 1456 cm^{-1} $CH_2\delta$
Na_2CO_3	1078 cm^{-1} ϑ_1

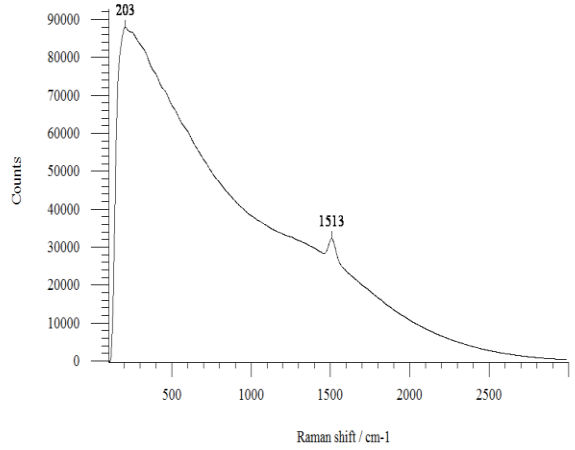

Figure 21 (a): Raman Spectra of floc

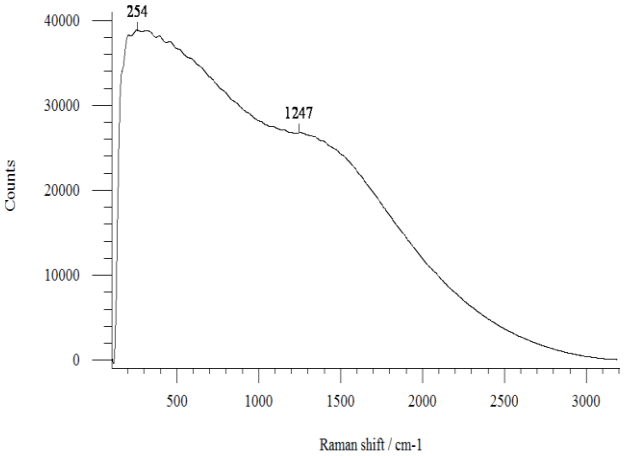

(b) Raman Spectra of floc with turbidity 1

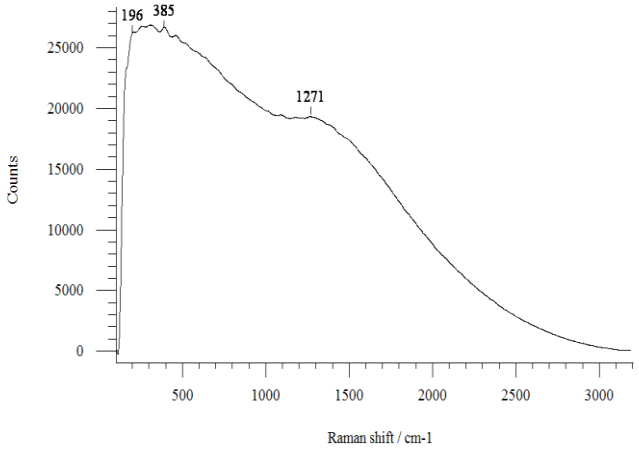

Figure 21 (c) Raman Spectra of floc with turbidity 1.6

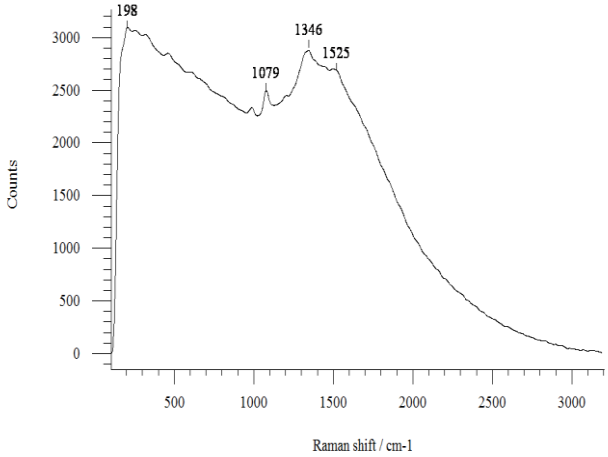

(d) Raman Spectra of floc with turbidity 2.5

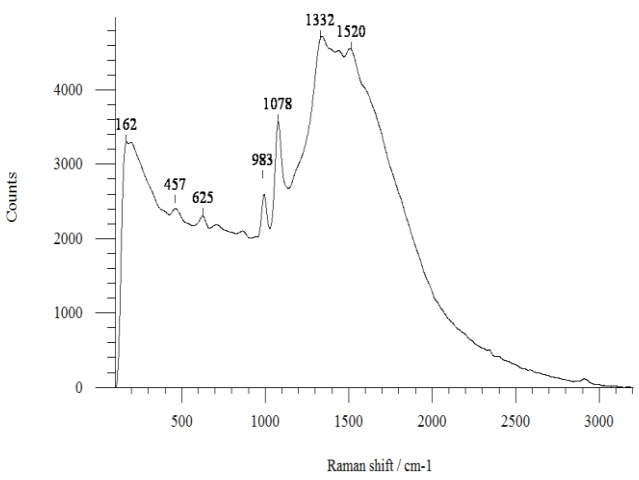

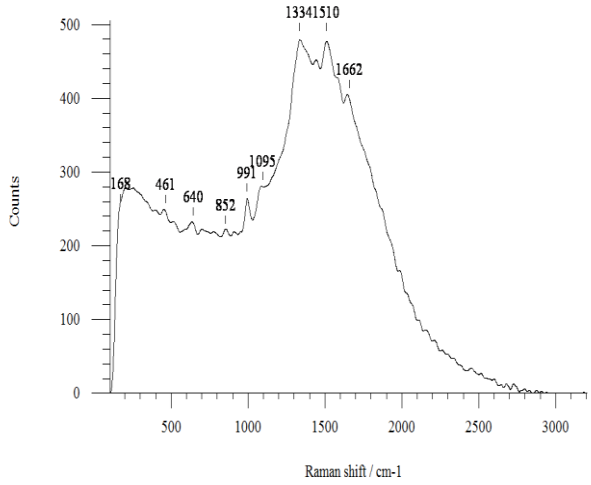

Figure 21 (e): Raman Spectra of PAM network of floc with turbidity 2.5

The raman spectra show only vibration modes of PAM and traces of clay. Hence we conclude that clay has masked the floc hence signature peaks of inorganic species are not seen. PAM

network engtangled all the clay and inorganic species. This is furthe verified by the digital microscopic images.

Images of floc taken by Digital microscope - *MightyScope 5.0 M (*Magnification 10x – 200x)

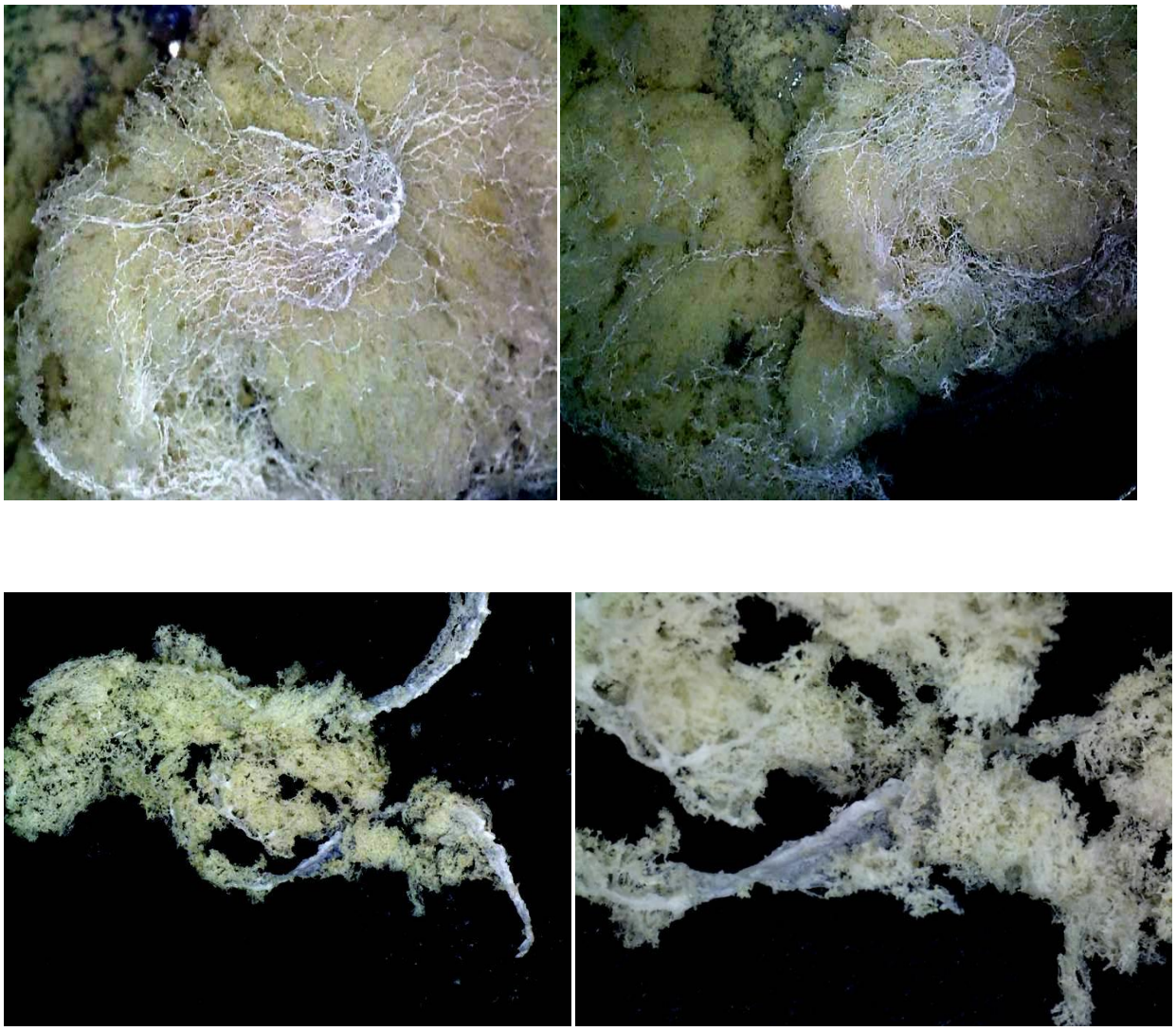

Figure 22 (a,b,c,d): Image of floc without arizona dust showing PAM network

4.2.3 EDX results

Three different floc samples are taken.

Sample A: Floc made without adding Polyacrylamide.

Sample B: Arizona dust is added in the floc formulation.

Sample C: Floc with Polyacrylamide and no Arizona dust. (Note that Arizona dust is added to increase the turbidity of the solution.)

Pellets of these samples of the size 1 cm x 1 cm x 2 mm are made using IR pelletizer.

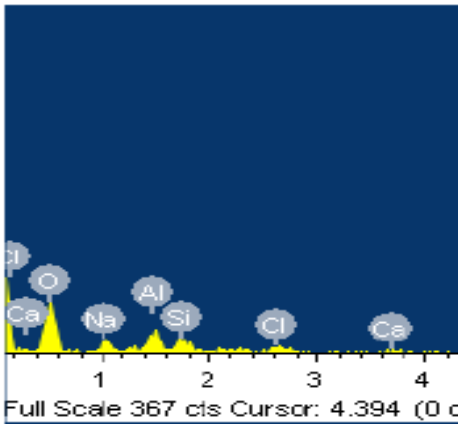

Element	Weight %	Atomic %
O K	55.68	68.93
Na K	9	7.76
Al K	12.93	9.49
Si K	10.88	7.67
Cl K	7.26	4.06
Ca K	4.24	2.10
Total	100	

EDX for floc sample A

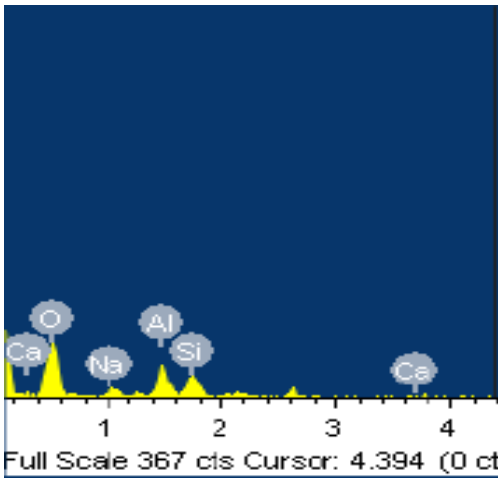

Element	Weight %	Atomic %
O K	57.25	69.17
Na K	5.75	4.83
Al K	18.54	13.28
Si K	18.47	12.71
Ca K	0.0	0.0
Total	100	

EDX for floc sample B

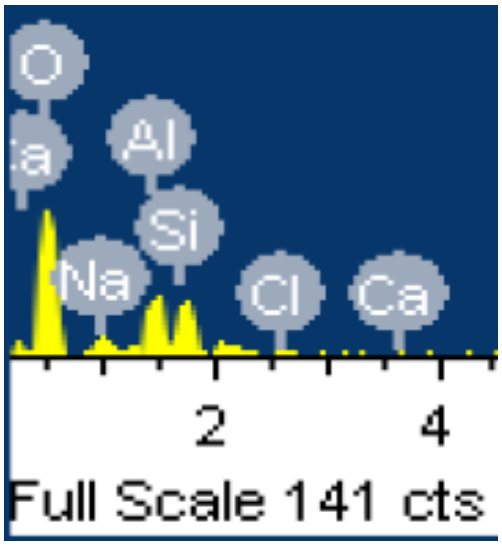

Element	Weight %	Atomic %
O K	60.68	72.69
Na K	3.21	2.67
Al K	15.85	131.26
Si K	17.16	11.71
Cl K	3.09	1.67
Ca K	0.0	0.0
Total	100	

EDX for floc sample C

In EDX since the penetration depth of the incident electron beam is of the order of 1000 microns and more, inorganic species like Al, Ca could be seen.

4.2.4 XPS results:

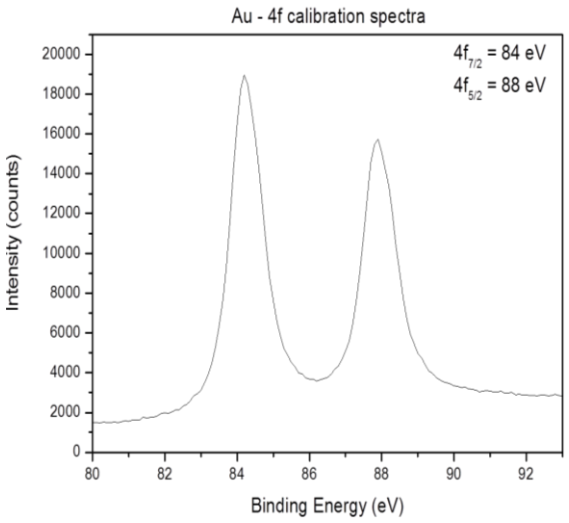

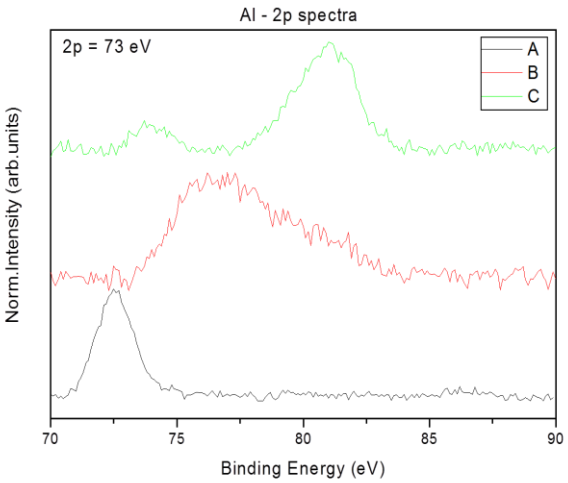

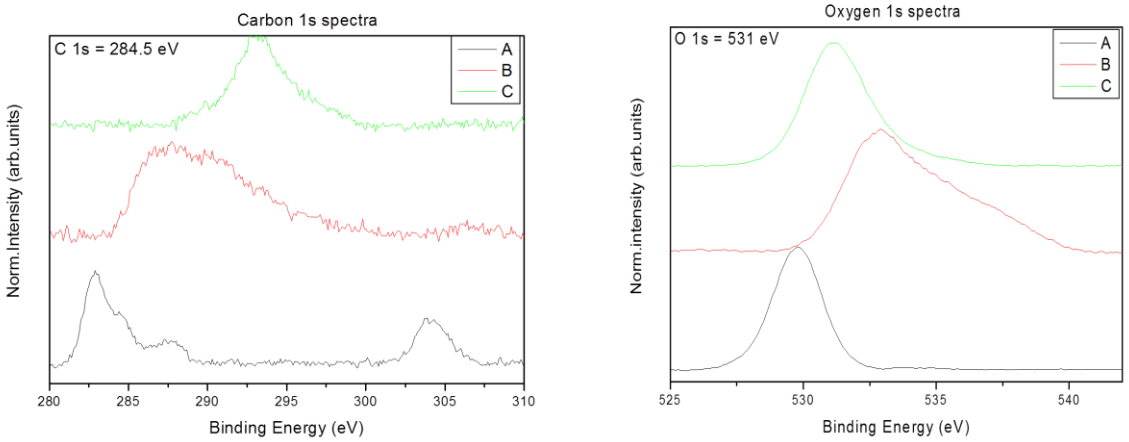

XPS data suggests that the surface species are predominantly carbon, oxygen i.e. PAM network. The corelevels of inorganic species are very broad suggesting that they are covered by other species.

4.3 Conclusions:

Comprehensive characterization of aluminum flocs was done in the context of drinking water.

The physical characterization of flocs suggests that:

- flocs can withstand extreme cases of hardness or softness (TDS) of water. This has been confirmed by fractal dimension data. D_f values also suggest the maximum and minimum pH conditions of the solution at the flocs can form. Optimum pH and TDS conditions for effective floc formation are at pH =6 and TDS = 350 ppm.
- Floc behaviour was studied at a different shear rate and optimum rate was tested. Floc growth, breakage and re-growth observed and correlated with D_f.
- Compactness of floc was tested by fractal dimension calculations under different shear conditions.

The chemical characterization of flocs showed that the sweeping mechanism by PAM is predominant over charge neutralization by aluminum salt. Aluminum species is not found on the surface as the EDS spectra of aluminium is very broad. Other species like PAM network and clay have masked the Al species.

Discussion

Coagulants are used to remove impurities from polluted water. The most common coagulants used in water purification are "Alums". **Alums** are double salts of sulfate with the formula $AM(SO_4)_2 \cdot 12H_2O$,where A is a monovalent cation such as potassium or ammonium and M is a trivalent metal ion such as aluminium or chromium(III). Coagulation by metal salts is an important and widely applied process in water and wastewater treatment. In our experiment we use aluminium salts, because of its effectiveness in treating a wide range of water types at a relatively low cost. On the basis of conventional aluminum salts ($AlCl_3$ and alum), the researches on prehydrolyzed aluminum coagulants have developed rapidly in the recent years. Prehydrolyzed aluminum coagulants have many advantages over conventional aluminum salts including less sludge production and less dependence on temperature and pH. Aluminium Sulfate hexadecahydrate ($Al_2(SO_4)_3.16\ H_2O$) contains a range of pre-formed Al(III) hydrolysis species with superior quality and structure, which are fairly stable for further hydrolysis, resulting in higher coagulation efficiency.

Previous studies showed that the coagulation performance and the coagulation mechanism of aluminum salts are largely dependent on the Al (III) hydrolysis species in Aluminium Sulfate. Lower dosages are required to achieve water treatment goals, less chemical residuals are produced, resulting in lower final TDS. Aluminium salts when added to the solution immediately dissociate to form hydrated products like $Al(H_2O)_6^{3+}$. These species are referred to as trivalent ions of aluminium and are often represented as Al^{3+}.

The formation of these species depends highly on the pH of the solution hence varying pH has a great effect on the hydroxide precipitate formation. The net charge on the molecule is affected by pH of its surrounding environment and can become more positively or negatively charged due to the gain or loss, respectively, of protons (H^+). The isoelectric spoint, sometimes abbreviated to **IEP**, is the pH at which a particular molecule or surface carries no net electrical charge. Surfaces naturally charge to form a double layer. In the common case when the surface charge-determining ions are H^+/OH^-, the net surface charge is affected by the pH of the liquid in which the solid is submerged.

The pI value (pH at iso-electric point) can affect the solubility of a molecule at a given pH. Such molecules have minimum solubility in water or salt solutions at the pH that corresponds to

their **pI** and often precipitate out of solution. The IEP for aluminium is around six. Hence at pH below six, aluminium is positively charged and at a higher pH it is negatively charged. Mechanism involved in coagulation using aluminium salts is charge neutralization. Since most colloidal particles, in our case bentonite clay, are negatively charged, positively charged Aluminium species gets attracted to them resulting in charge neutralization. Thus at pH below pI stable colloids exist. As pH is increased towards pI, the stability decreases and the particles can aggregate into larger aggregates. It is worth noting that the IEP for $Al(OH)_3$ occurs at Aluminum speciation, which refers to the partitioning of aluminum among different physical and chemical forms, and aluminum solubility are affected by a wide variety of environmental parameters, including pH, solution temperature, dissolved organic carbon (DOC) content, and the presence and concentrations of numerous ligands. Metals in solution may be present as dissolved complexes, as "free" or aquo ions, in association with particles, as colloids or as solids in the process of precipitating.

There are two general types of ligands that can form strong complexes with aluminum in solution. Inorganic ligands include anions such as sulphate (SO_4^{2-}), fluoride (F^-), phosphate (PO_4^{3-}), bicarbonate (HCO_3^-) and hydroxide (OH^-), among others. The relative concentrations of the inorganic and organic ligands generally determine the proportions and type of complexes that are formed in solution.

Aluminum is a strongly hydrolysing metal and is relatively insoluble in the neutral pH range (6.0-8.0) (Figure 23). In the presence of complexing ligands and under acidic (pH < 6) and alkaline (pH > 8) conditions, aluminum solubility is enhanced. At low pH values, dissolved aluminum is present mainly in the aquo form (Al^{3+}). Hydrolysis occurs as pH rises, resulting in a series of less soluble hydroxide complexes (e.g., $Al(OH)^{2+}$, $Al(OH)^{2+}$). Aluminum solubility is at a minimum near pH 6.5 at 20°C and then increases as the anion, $Al(OH)_4$, begins to form at higher pH. Thus, at 20°C and pH < 5.7, aluminum is present primarily in the forms Al^{3+} and $Al(OH)^{2+}$. In the pH range 5.7 to 6.7, aluminum hydroxide species dominate, including $Al(OH)^{2+}$,and then $Al(OH)_3$. Typically, at a pH of approximately 6.5, $Al(OH)_3$ predominates over all the other species. In this range, aluminum solubility is low, and availability to aquatic biota should also be low. At pH > 6.7, $Al(OH)_4^-$ becomes the

dominant species. Aluminum-hydroxide complexes predominate over aluminum-fluoride complexes under alkaline conditions.

Mononuclear aluminum hydrolytic products combine to form polynuclear species in solution. Aluminum begins to polymerize when the pH of an acidic solution increases to over 4.5:

$$2Al(OH)(H_2O)_5^{2+} \rightleftharpoons Al_2(OH)_2(H_2O)_8^{4+} + 2H_2O$$

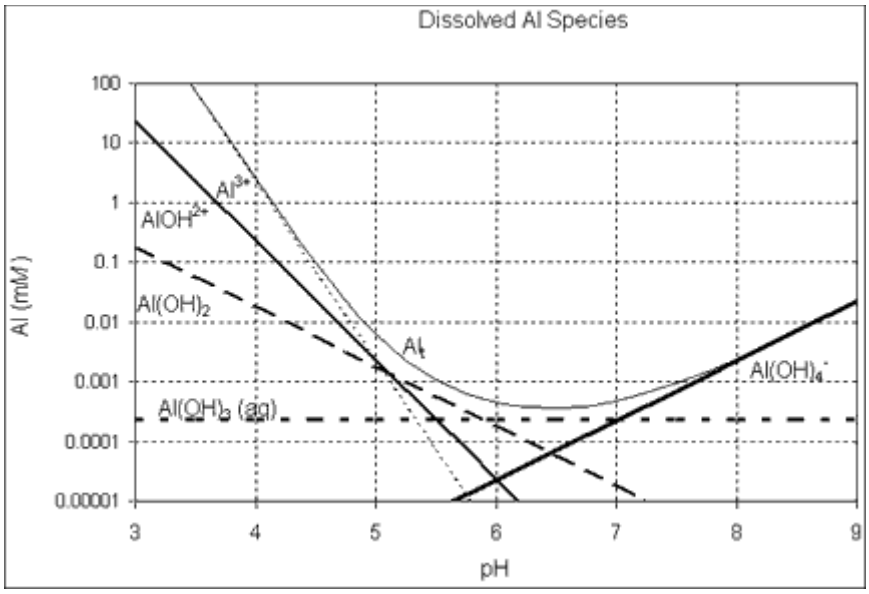

Figure 23: Solubility curve of aluminum species and total aluminum, Al_t in relation to pH in a system

REFERENCES

1. **World Health Organization**. Guidelines for drinking-water quality Vol. 1, Recommendations. – 3rd ed.
2. On flocculation of particles. E.W. Hilgard. American Journal of Science **March 1879** vol. Series 3 Vol. 17 no. 99 **205-214**

3. Coagulation in drinking water treatment-Particles, Organics and Coagulants. JK Edzwald. Water Science and Technology 1993 Vol. p. 27 21-35.

4. O'Melia CR, Tiller CL. Physicochemical aggregation and deposition in aquatic environments. In: Buffle J, Leewenvan HP, editors. Environmental particles, vol. 2. Boca Raton, FL: Lewis Publishers, 1993. p. 353–86 (Chapter 8).

5. Elimelech M, Gregory J, Jia X, Williams RA. Particle deposition and aggregation—measurement, modeling and simulation. Butterworth-Heinemann Ltd., London, UK 1995.

6. Chakraborti RK, Atkinson JF, Van Benschoten JE. Characterization of alum floc by image processing. Environ SciTechnol 2000;34 (18):3969–76.

7. Jiang Q, Logan BE. Fractal dimensions of aggregates determined from steady state size distributions. Environ SciTechnol 1991;25 (12):2031–8.

8. Jiang Q, Logan BE. Fractal dimensions of aggregates from shear devices. J Am Water Works Assoc 1996; 88 (2):100–13.

9. Logan BE, Kilps JR. Fractal dimensions of aggregates formed in different fluid mechanical environments. Water Res 1995;29 (2):443–53.

10. Gardner KH. Kinetic models of colloid aggregation. In: Hsu JP, editor. Interfacial forces and fields: theory and applications. New York: Marcel Dekker, Inc., 1999. p. 509–50.

11. Fractal Geometry of Colloidal Aggregates. Dale W. Schaefer, James E. Martin, Pierre Wiltzius, and David S. Cannell. Phys. Rev. Lett. 52, 2371 – Published 25 June 1984

12. Fractal Geometry of Particle Aggregates Generated in Water and Wastewater Treatment Processes. Da-hong Li and Jerry Ganczarczyk'. Environ. Sci. Technoi., Vol. 23, No. 11, 1989.

13. On techniques for the measurement of themass fractal dimension of aggregates G.C. Bushella, D.Woodfielda, J. Raper c, R. Amala. Advances in Colloid and Interface Science 95 (2002) 1-50.

14. Flocculation: A New Way to Treat the Waste Water. TridibTripathy and BhudebRanjan De. Journal of Physical Sciences, Vol. 10, 2006, 93 – 127.

15. J.M. Montgomery, Water Treatment: Principles and Design, John Wiley and Sons, New York, 1985,116.

16. J. Gregory, Flocculation of Fine Particles in Innovation in Flotation Technology, P. Mavrosand K.A.Matis eds., Kluwer Academic Publishers, Netherlands, 1992.101.

17. H.R. Kruyt, Collid Science, Vol.1, Elsevier, New York, 1952.

18. A.K.Banerjee, W.W Tscharnuter, B.B Weiner, and Y.B Gokhale, Measuring Zeta Potential Using Light Scattering, Chemical Industry Digest, 116,4th Quarter, December, 1996.

19. A Gouy–Chapman–Stern model of the double layer at a (metal)/(ionic liquid) interface Keith B. Oldham * Journal of Electroanalytical Chemistry 613 (2008) 131–138

20. Stern, O. *Z.Electrochem*, 30, 508 (1924)

21. G.R Rose. and M.R St.John., Flocculation in Encyclopedia of Polymer Science and Engineering, (H.F.Mark, N.M.Bikales, C.G.Overberger, Georg Menges and J.I.Kroschwitz,eds.) John Wiley & Sons, New York, Vol.7 p.211, 1987.

22. J.Gregory, Flocculation by Polymers and Polyelectrolytes, in Solid-Liquid Dispersions (Th.F. Tadros, ed.), Academic Press (London) Ltd., Ch.8, 1987.

23. B.V. Deryagin, and L.D Landau Theory of the Stability of Strongly Charged Lyophobic Sols and the Adhesion of Strongly Charged Particles in Solutions of Electrolytes, ActaPhysicochim URSS 14, (1941)733 .

24. E.J.W Verway. and G. Overbeek J.Th., Theory of Stability of Lyophobic Colloids, Elsevier, Amsterdam, 1948.

25. DLVO Interaction between Colloidal Particles: Beyond Derjaguin's Approximation *Subir Bhattacharjee,* Croatia Chemicaacta**71** (4) 883-903 (1998)

26. Application of the DLVO theory for particle deposition problems. Zbigniew AdamczykUet. al. Advances in Colloid and Interface Science 83 (1999) 137-226.

27. Riddick, M.Thomas Zeta Potential and its Application to Difficult Waters, JWWA, (1961),1007.

28. Guan, J., Waite, T.D. and Amal, R. (1998).Rapid structure characterization of bacterial aggregates. Environmental Science&Technology, 32, 3735–3742.

29. Bushell, G.C., Yan, Y.D., Woodfield, D., Raper, J. and Amal, R. (2002). On techniques for the measurement of the mass fractal dimension of aggregates. Advanced of Colloid Interface Science, 95, 1–50.

30. Gardner KH. Kinetic models of colloid aggregation. In: Hsu JP, editor. Interfacial forces and fields: theory and applications. New York: Marcel Dekker, Inc., 1999. p. 509–50.

31. Yeung, A.K. and Pelton, R. (1996). Micromechanics: a new approach to studying the strength and breakup of flocs. Journal of Colloid Interface Science, 184, 579–585.

32. Jarvis, P., Jefferson, B. and Parsons, S.A. (2005a). How the natural organic matter to coagulant ratio impacts on floc structural properties. Environmental Science & Technology, 39, 8919-8924.

33. Chromatography/Fourier transform infrared spectroscopy and its applications, by Robert White, p7.

34. S. P. S. Porto, J. A. Giordmain and T. C. Damen, Phys. Rev. **147**, 608 (1966).

35. Russ, J. C. (1984) Fundamentals of Energy Dispersive X-ray Analysis, Butterworths, London.

36. X-ray photoelectron spectroscopy **Jack M. Hollander , William L. Jolly**.Acc. Chem. Res., **1970**, 3 (6), pp 193–200 principle 1,2. 17-119

37. Keck C.M., Muller R.H, Int. J. Pham. 355, p. 150-163, 2008.

38. ISO 13320: 2009 Particle size analysis – Laser diffraction methods.

39. Guinier A: Fournet, G.; Walker, C. L.; Yudowitch, K. L. Small Angle Scattering of X-rays. Wiley New York, 1995.

40. Lin, M. Y.; Klein, R.; Lindsay, H. M.; Weitz, D. A.; Ball, R. C.; Meakin, P. J. Colloid Interface Sci. **1990**, 137, 263-280.

41. Logan, B. E.; Wilkinson, D. B. Limnol. Oceanogr. **1990**, 35, 130-136.

42. **Influence of pH on Flocs Formation, Breakage and Fractal Properties — The Role of Al13 Polymer** WeiyingXu, BaoyuGao*, QinyanYue, Xiaowen Bo. *Journal of Water Sustainability*, Volume 1, Issue 1, June 2011, 45–57